REVIEW

Check for updates

Earth-abundant non-toxic perovskite nanocrystals for solution processed solar cells

Sergio Aina, [ID] [ab] Belén Villacampa [ID] [ac] and María Bernechea [ID] *[abde]

Semiconductor nanocrystals, used in quantum dot solar cells, are interesting materials for photovoltaics because they can be obtained in solution and can be composed of abundant elements. Moreover, as compared to other photovoltaic materials, nanomaterials show unique features due to their novel size- and shape-dependent properties such as band gap tuning, multiple exciton generation, and modulation of n- or p-type behaviour by doping or by modifying the ligands on the surface of the nanocrystals. Quantum dot solar cells, together with perovskite solar cells, are the latest incorporation to photovoltaic technologies and have already shown impressive progress in efficiencies and great promise as alternatives to commercial solar cells. However, in all cases, the highest efficiencies are obtained with materials that contain lead in their composition. To solve the problem of toxicity, several materials have been proposed as substitutes. In this review, we summarize some of the non-toxic alternatives that have been synthesized as nanocrystals and incorporated in photovoltaic solar cells, specifically: tin (Sn), germanium (Ge), bismuth (Bi), and antimony (Sb)-based materials. Our findings show that this field has been scarcely covered; there are very few reports on non-toxic perovskite nanocrystals incorporated in solar cells and in general, the efficiencies are still modest. However, this area deserves more attention since some nanocrystal-based solar cells already outperform bulk counterparts. For each case, we also discuss factors limiting efficiency, the approaches followed to overcome these limitations, and the possible solutions to improve efficiency.

Introduction

In the last 10 years, two new types of photovoltaic solar cells have emerged: perovskites and quantum dots (QDs), also known as colloidal semiconductor nanocrystals (NCs). Starting from modest efficiencies around 3%, they have quickly escalated up to 25.5 and 18.1%, respectively, in this short period of time.[1] In both cases, the active materials are composed of earth-abundant elements and can be processed from solutions, which offers easier manufacture and lower prices than commercial solar cells. Therefore, they might soon become an alternative to commercial solar cells, whether alone or in tandem with other photovoltaic technologies.

Semiconductor nanocrystals are nanomaterials with typical dimensions of less than 10 nm. They offer interesting and

[a] *Instituto de Nanociencia y Materiales de Aragón (INMA), CSIC-Universidad de Zaragoza, Zaragoza, 50009, Spain. E-mail: mbernechea@unizar.es*

[b] *Department of Chemical and Environmental Engineering (IQTMA), University of Zaragoza, 50018 Zaragoza, Spain*

[c] *Department of Condensed Matter Physics, University of Zaragoza, 50009 Zaragoza, Spain*

[d] *Networking Research Center on Bioengineering, Biomaterials and Nanomedicine (CIBER-BBN), 28029, Madrid, Spain*

[e] *ARAID, Government of Aragón, 50018 Zaragoza, Spain*

unique properties for their use in several optoelectronic devices and more precisely in solar cells. Traditional photovoltaic materials have a fixed band gap that determines the range of photons that solar cells will be able to absorb. However, the reduced size of nanocrystals leads to quantum confinement effects, *i.e.* their electrical and optical properties, including band gap, can be easily modified just by changing their shape and size (Fig. 1A). Multiple exciton generation (MEG), the generation of two (or more) electron–hole pairs from one absorbed high-energy photon, is more efficient in nanocrystals than in bulk semiconductors and this could produce efficiencies over the theoretical limit for single-junction solar cells (Shockley–Queisser limit).[2,3] Moreover, their behaviour as n- or p-type semiconductors and doping density can be modified by introducing foreign atoms, like in traditional silicon technologies, and also by surface treatments. Nanocrystals are stabilized in solution thanks to the presence of long chain ligands on their surface that are replaced by shorter ligands or atoms during the fabrication of solar cells (Fig. 1B). Depending on the final ligands on the surface of NCs the position of the Fermi level and/or the valence and conduction bands can be modified, which is a unique feature of nanocrystals and a very powerful tool (Fig. 1C).[4] Taking advantage of all these features efficiencies over 16% have been obtained using perovskite nanocrystals ($Cs_{1-x}FA_xPbI_3$).[5]

Fig. 1 (A) Scheme showcasing the band gap tunability in nanocrystals as a function of their size. (B) Scheme of a surface ligand exchange process where long chain capping molecules are replaced by shorter ligands. (C) Diagrams representing the shift of the valence and conduction bands (left) or the Fermi level (right) depending on the nature of ligands on the surface of the NCs (L1, L2, L3...). (D) Perovskite ABX_3 structure. X site corresponds to a halide anion, A site to an organic (MA, FA...) or inorganic (Cs, Rb...) cation, and B (green sphere) to a metal (Pb, Sn, Ge...) cation. (E) Schematic representation of 0D, 1D, 2D, and 3D perovskite structures.

Perovskite solar cells (PSC) are based on materials with a general formula ABX_3; where X is a halide anion (X = Cl, Br, I), B is an inorganic cation (usually Pb), and A can be an inorganic (usually Cs or Rb), or an organic cation (usually MA = methylammonium, or FA = formamidinium) leading to all-inorganic or hybrid organic–inorganic perovskites, respectively (Fig. 1D).[6] They usually crystallize in a 3D structure, however, the dimensionality can change to 2D, 1D, or 0D (Fig. 1E) if Pb is replaced in the B position by a cation with a different charge (Cu^+, Sb^{3+}, Sn^{4+}), which may consequently alter the perovskite formula (e.g. $A_2B_2X_6$, $A_3B_2X_9$). Additionally, the structure can also be modified depending on the volume of cation A (greater volumes can lead to distortions in the 3D structure) or the radius of the B atom (for example, Cu smaller radius favours 2D structures).[7] In general, the fabrication of the active layer is performed by mixing the precursors in solution, depositing the solution on a substrate followed by a final thermal treatment, usually at low temperatures (<100 °C). This implies that, in these devices, synthesis, film deposition, and grain crystallization occur at the same time.

The best performing perovskite solar cells are based on lead-containing materials (Pb^{2+} cations in B position). They have high absorption coefficients, suitable direct band gaps (around 1.5–2.5 eV), small exciton energy, balanced and long charge-carrier diffusion-length, high carrier mobility, and trap-free carrier relaxation, which favour high efficiencies and make them ideal for photovoltaic applications.[6,8–10] However, the long-term stability of lead-perovskite solar cells is poor, affected by moisture, oxidation, heat, or light, which causes losses in the

efficiency of the devices over time when working at ambient conditions.[11] For instance, $MAPbI_3$ degrades into PbI_2 and MAI in the presence of water, and high temperatures (150 °C) can also induce the perovskite material degradation.[12–16]

It has been proposed that the key feature that makes lead-based perovskites such great materials for photovoltaic applications is their defect tolerant nature, associated with the $6s^2$ lone pair configuration of Pb^{2+} that leads to large dielectric constants, small effective masses, a valence band maximum composed of antibonding states, and high levels of band dispersion.[10,13,17,18] Following this rationale, perovskite materials composed of other ns^2 cations, such as Sn^{2+}, Ge^{2+}, Sb^{3+}, and Bi^{3+}, have been proposed as alternatives for their use in solar cells, as they may offer similar attractive properties than lead-perovskites, but better stability in ambient conditions.[10,13] Moreover, lead is a toxic heavy metal that dissolves in water and tends to bioaccumulate, which is problematic during fabrication, use, and disposal of lead-based devices.[19–21] The suggested alternative cations are considered more benign than lead, or, like bismuth, non-toxic elements; therefore, they offer the additional advantage of eliminating health or environmental concerns. Indeed, these materials may be an attractive option for devices in close contact with humans, such as wearables or indoor applications.[22–24]

In the last years, there has been some progress in this area and some reviews have already summarised the most relevant results in lead-free bulk perovskite materials for solar cells.[10,13,15,18,21,25–32] In this review, we focus on Sn^{2+}, Ge^{2+},

Bi^{3+}, and Sb^{3+} perovskites that have been synthesized as nanocrystals and incorporated in photovoltaic solar cells. Some recent reviews have focused on the synthesis and light emission properties of lead-free perovskite NCs, but none of them has collected the efficiencies obtained incorporating the nanocrystals in solar cells.[33–35]

Perovskite nanocrystals for solar cells

Colloidal perovskite nanocrystals offer similar defect tolerance as bulk perovskite materials plus additional advantages related to nanoscale phenomena such as modification of the properties by changing the size or shape of the nanocrystals, multiple exciton generation features and, property-tuning by modifying the ligands on the surface, which at the same time could improve device stability by passivating surface defects. Additionally, the decoupling of material synthesis and material deposition simplifies fabrication and allows to prepare phases or compositions that are not stable in the bulk as well as better control on the stoichiometry when compared to the *in situ* preparation of bulk perovskites.[2–4]

The most common structure of a perovskite solar cell, also used in the perovskite nanocrystal solar cells, consists of an n–i–p junction (n-type, intrinsic, and p-type semiconductors). The light harvester layer (intrinsic semiconductor) is placed between a Hole Transport Layer (HTL, p-type semiconductor), an Electron Transport Layer (ETL, n-type semiconductor), and the two metallic contacts (Fig. 2A). Alternatively, NCs can be introduced in Dye Sensitized Solar Cells (DSSC). In a typical DSSC, upon light absorption the excited sensitizers inject electrons into the conduction band (CB) of TiO_2. The oxidized dyes are regenerated by the electrolyte (Fig. 2B). NCs can be incorporated acting as sensitizers, either alone or in combination with other dyes to enhance light absorption.

The solar cell performance of Pb-perovskite NCs has progressed significantly from the first work by Kojima *et al.* in 2009 reporting an efficiency of 3.8% using $MAPbI_3$ NCs as sensitizers in DSSCs.[36] Two years later, it was found that by optimizing the thickness of the TiO_2 layer, the efficiency could increase up to 6.5% for $MAPbI_3$ NCs. Nonetheless, the perovskite layer was only stable for 10 minutes until the NCs dissolved in the electrolyte.[37] Later, substituting the electrolyte by spiro-OMeTAD, acting as HTL, the efficiency achieved was 9.7%.[38] In the field of all-inorganic perovskites, (without volatile components, detrimental in terms of stability) the use of colloidal NCs has allowed to stabilize structural phases desirable for photovoltaics. For instance, the cubic α-$CsPbI_3$ form has an optimal bandgap for photovoltaic applications, but it is hardly achievable in bulk, where the orthorhombic δ form prevails below 320 °C. By using ligands such as oleic acid and oleylamine, α-$CsPbI_3$ NCs were synthesized and stabilized at room temperature, and an efficiency of 10.77% was reported for perovskite NCs solar cells.[39] The introduction of a polymer in the interface between the NCs and the HTL allowed to adjust the energy levels and consequently to enhance charge extraction. Efficiency values as high as 14% and 13.2% have been obtained for $CsPbI_3$ and $FAPbI_3$ NCs perovskite cells, respectively.[40]

Nowadays, $Cs_{0.5}FA_{0.5}PbI_3$ NCs have delivered the highest published efficiency for nanocrystal-based PSC with a 16.6%, where FA addition played an essential role by reducing non-radiative recombination.[5] The record for all-inorganic nanocrystal-based PSC is 16.07% obtained with Zn-doped $CsPbI_3$ NCs.[41] The optimization between energy levels, doping with other elements, or the introduction of stabilizing ligands/molecules have been essential for the development of devices with greater efficiencies.

Non-toxic perovskite nanocrystals for solar cells

Despite the high efficiency values achieved with lead-based perovskite NCs[5] the stability and toxicity issues commented above have led to the proposal of several non-toxic materials to substitute them. The main non-toxic perovskite substitutes are composed of tin, germanium, bismuth, and antimony. Tin and germanium are the obvious alternatives to lead-based perovskites since they belong to the same group in the periodic table and they share analogous electronic configurations. Therefore, similar properties and crystalline structures are expected for these Pb-free perovskites. Moreover, they are relatively abundant on earth crust and considered as less toxic than lead. However, tin and germanium show a higher tendency to oxidize (from Sn^{2+} and Ge^{2+} to Sn^{4+} and Ge^{4+} cations) than Pb^{2+}, a fact explained by the inert pair effect. Lead has the strongest inert pair effect, which means that its outermost ns^2 electrons ($6s^2$) are strongly bound to the nucleus due to the poor shielding of d and f orbitals. As the atomic number increases, the attraction force of the nucleus over
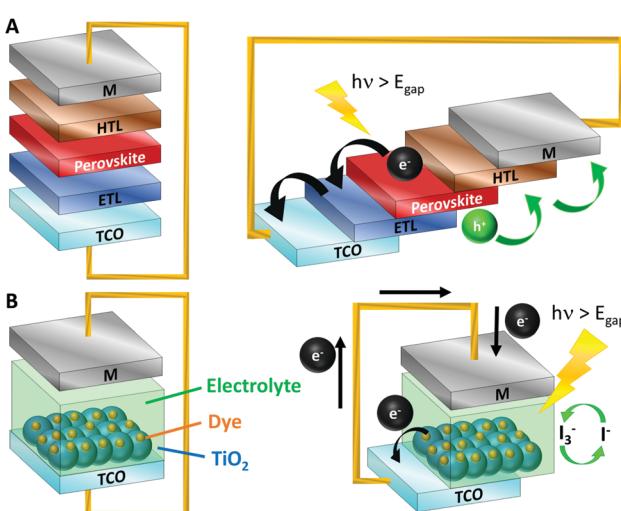

Fig. 2 (A) Left: n–i–p structure in perovskite solar cells. The perovskite material acts as light harvester, HTL and ETL are the hole and electron transport layers, respectively, M is the metallic contact, and TCO the transparent contact layer. Right: Charges flow in the structure (B) Left: Typical DSSC structure consisting of mesoporous TiO_2 layer with adsorbed dye molecules, electrolyte (iodide/triiodide in this example), and metallic (M) and transparent contacts (TCO). Right: Charges flow in the structure.

the electrons is usually greater, as well as the shielding due to the higher number of energy levels. However, d and f electrons shielding effect is weak; therefore, the interaction between the $6s^2$ electrons and nucleus is stronger than expected, preventing their participation in any bonding. For that reason, the most stable form for lead is Pb^{2+}, not Pb^{4+}. In the case of tin, this inert pair effect is reduced because the $5s^2$ electrons are not as strongly tighten as $6s^2$ in Pb, which favours Sn^{2+} oxidation to Sn^{4+}. Germanium is upper in the group, which makes the inert pair effect even weaker, $4s^2$ electrons are more likely to participate in chemical bonding and Ge^{2+} cations tend to oxidize to Ge^{4+}.[10,35,42–44] Being adjacent to Pb^{2+} and Sn^{2+} in the periodic table, Bi^{3+} and Sb^{3+} have similar ns^2 electronic configuration, are more stable in ambient conditions, have demonstrated low toxicity, and are relatively abundant on the earth crust. Apart from the similar electronic configuration, Bi and Sb can be incorporated into the perovskite lattice because they have an ionic radius similar to Pb. However, in some cases, due to their different oxidation state (+3), they form low dimensionality (2D, 1D or 0D) structures in order to maintain charge neutrality. This may cause problems in charge transport and have a significant impact in the efficiency of devices.[13,21,26,27,35]

The next sections are organized as follows: first, characteristics of each material, application in bulk solar cells, and maximum efficiencies obtained are summarized. Finally, a detailed review of the corresponding perovskite NCs used in solar cells and their efficiencies (also referred as power conversion efficiency, PCE) are explained. We have observed that there are very few examples of perovskite NCs introduced as absorbing material in solar cells, therefore, in some cases, we have included materials that may not form the traditional lead-halide composition or the typical perovskite crystalline structure, but that share the main characteristics of perovskite materials used in solar cells.

Tin-based perovskites

Tin (Sn) is the natural alternative to lead-perovskite NCs. Sn is a non-toxic element that belongs to the same group in the periodic table as Pb and Ge. They have analogous electronic configurations; thus, they form similar compounds and similar properties are expected. However, as mentioned above, Sn^{2+} cations are unstable because they tend to oxidize to Sn^{4+}. This oxidation process creates undesired vacancies in the crystalline structure that favours carrier recombination, which may result in low photoluminescence quantum yield (PLQY) and solar cell efficiency.[33,45,46]

The interest in substituting lead has fostered the use of several tin-based materials as absorption layers in bulk perovskite solar cells. For example, optimized all-inorganic $CsSnI_3$ solar cells have shown a 4.81% power conversion efficiency,[47] recently improved up to 7.5% by incorporating N,N'-methylenebis (acrylamide) into the perovskite layer.[48] $FASnI_3$ perovskite solar cells treated with SnF_2–pyrazine showed an efficiency of 4.8%, maintained over 100 days,[49] which was later improved up to 9% when mixing the 3D $FASnI_3$ perovskite with a small quantity of the 2D Sn-perovskite PEA_2SnI_4 (PEA = phenylethylammonium). Apparently, the addition of the 2D material promotes the growth

of highly crystalline and oriented $FASnI_3$ grains which reduces the number of grain boundaries, suppresses tin vacancies, and improves charge carrier lifetime.[50] Moreover, applying a passivation treatment with edamine (EDA), $FA_{0.98}EDA_{0.01}SnI_3$ bulk perovskite solar cells achieved a 10.18% efficiency. Edamine molecules prevented the charge carrier recombination by suppressing tin oxidation and iodide vacancies.[51] Recently this value has been improved up to 13% by employing GeI_2 doped $(FA_{0.9}EA_{0.1})_{0.98}$ $EDA_{0.01}SnI_3$, where EA corresponds to ethylammonium cations. The presence of EA in the perovskite enhanced the charge transport by presenting more favourable energy level adjustment between the perovskite and the charge transport layers.[52] Also, other hybrid organic–inorganic Sn-perovskites have been tested in devices: ethylenediammonium–$MASnI_3$ solar devices delivered a 6.63% efficiency.[53] Mixing methylammonium and formamidinium a power conversion of 8.12% was achieved for $FA_{0.75}MA_{0.25}SnI_3$ devices.[54]

Tin-based materials tend to suffer from bulk recombination due to the presence of Sn vacancies generated by Sn^{2+} oxidation, which strongly limits their properties as light absorbers. In order to prevent Sn^{2+} oxidation, additives such as SnI_2 excess[47] or pyrazine[49] have been introduced. Another option has been the use of the most stable tetravalent cation (Sn^{4+}).[55,56] However, Sn^{4+}-based perovskites offer lower efficiencies (1%), as shown in studies employing Cs_2SnI_6.[45,56,57] Therefore, the key for achieving better performing devices might rely on the control of Sn^{2+} oxidation. The use of hypophosphorous acid (HPA) has shown to increase the efficiency of a $CsSnBr_2I$ perovskite solar cell from 1.67% to 3%. The HPA addition induced the formation of perovskite seeds and decreased recombination by lowering carrier mobility and charge carrier density. Moreover, devices showed excellent stability. Experiments under 1 sun at maximum power point showed a 98% retention of the original efficiency, even at temperatures as high as 200 °C, while in analogous experiments $MAPbI_3$ devices lost almost 90% of the original efficiency at temperatures of 80 °C. Furthermore, encapsulated devices stored under ambient conditions (25 °C and uncontrolled moisture) maintained $\approx$100% of the initial efficiency over a period of 77 days.[45]

Lately, tin-perovskite NCs have risen as alternatives to bulk tin PSC. They offer the general advantages of nanocrystals such as easy synthesis, quantum confinement and high photoluminescence yield.[33,58,59] Nevertheless, the aforementioned drawback caused by Sn^{2+} oxidation could be fostered in the nanoscale due to the high surface/volume ratio. Therefore, stabilization of the nanocrystals is crucial. By controlling the synthesis, functionalizing the surface with ligands[60,61] and adding excess of SnX_2, more stable tin-perovskite nanocrystals, such as $CsSnX_3$ NCs, can be obtained.[33,47,53] Only a few reports, including $CsSnI_3$ NCs, rod shaped $CsSnX_3$ NCs (X = Cl, Br, I), and $CH_3NH_3SnBr_{3-x}I_x$ NCs ($MASnBr_{3-x}I_x$ NCs) describe the use of tin-perovskite NCs as light harvesters in solar cells.

$CsSnI_3$ nanocrystals

A one-pot synthesis method was used to produce $CsSnI_3$ NCs by a simple and mild process. CsI and SnI_2 were used as

precursors, and triphenyl phosphite (TPPi) was added as antioxidant solvent additive (ASA) to prevent Sn^{2+} oxidation to Sn^{4+} and the subsequent formation of vacancies in the perovskite lattice. Thanks to the addition of TPPi the nanocrystals solutions remained clear and stable for at least 90 days. The photovoltaic performance of $CsSnI_3$ NCs was compared with a bulk $CsSnI_3$ active layer using the solar cell structure depicted in Fig. 3A. The active layer was sandwiched between poly(3,4-ethylenedioxythiophene)polystyrene sulfonate (PEDOT:PSS), acting as hole transport layer, and [6,6]-phenyl-C61-butyric acid methyl ester (PCBM), acting as electron transport layer. The antioxidant agent TPPi showed to improve the performance of bulk-based and NCs-based $CsSnI_3$ solar cells (Fig. 3B). Bulk $CsSnI_3$ devices showed an efficiency of 0.022%, which was enhanced up to 1.202% when adding TPPi. For the NCs-based devices (with TPPi too), the average efficiency obtained was 4.13% with a maximum of 5.03%. In stability experiments the NCs solar cell outperformed the bulk one; its efficiency remained intact during 30 days, while it was constantly varying for the bulk device.[58]

These results highlight the importance of overcoming Sn^{2+} oxidation to reach better photovoltaic devices. Moreover, they show that the introduction of perovskite NCs could improve the efficiency and stability of devices. The NC-based device was better in every aspect than the corresponding bulk solar cell; nonetheless, the performance is still far from $CsPbI_3$ NCs devices, that have achieved an efficiency over 16%.[41]

$CsSnX_3$ nanocrystals (X = Cl, Br, I)

$CsSnX_3$ rod-shaped nanocrystals (quantum rods, QRs) were synthesized using an easy, fast and clean solvothermal method. The advantage of QRs over spherical nanocrystals is that for the same diameter QRs have bigger volumes leading to a higher per-particle absorbance cross-section and, additionally, their elongated shape is supposed to improve charge injection to transport layers, which can improve device performance.[62] In the reported synthesis SnX_2 and Cs_2CO_3 were used as precursors, octadecene, oleylamine and oleic acid as solvents, and, to enhance the growth of high-quality QRs, trioctylphosphine oxide (TOPO) and diethylenetriamine were added as capping agents.[63]
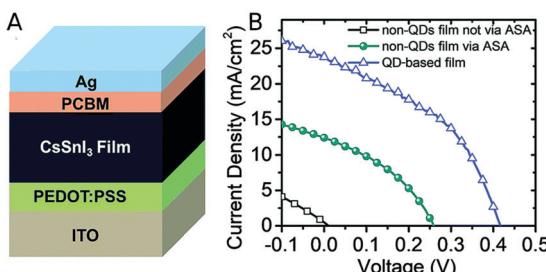
Fig. 3 (A) Device structure of the solar cell based on the $CsSnI_3$ films. (B) J–V curves of $CsSnI_3$ bulk solar cell (black), $CsSnI_3$ bulk solar cell with the addition of TPPi as antioxidant additive (green) and $CsSnI_3$ NCs solar cell with TPPi (blue). Reproduced from ref. 58 with permission from the Royal Society of Chemistry (RSC, Journal of Materials Chemistry A).

Table 1 Band gaps (E_g), approximated from PL emission peaks, and power conversion efficiency (PCE) of the solar cells fabricated with $CsSnX_3$ QRs. Extracted from ref. 63

	E_g (eV)	PCE (%)
$CsSnCl_3$	2.0	9.66
$CsSnBr_3$	1.9	10.46
$CsSnI_3$	1.7	12.96

A red shift in the band gap and PL emission, from 625 to 709 nm, was observed from the chloride to the iodide $CsSnX_3$ (X = Cl, Br, I) QRs (Table 1). The nanocrystals were used as absorbing layers in solar cells including TiO_2 as electron transport layer and spiro-OMeTAD as hole transport layer. The best efficiency was obtained for the $CsSnI_3$ QRs (Table 1), probably due to its more adequate band gap among the three materials. Additionally, the stability of $CsSnI_3$ QRs and bulk $MAPbI_3$ sealed solar cells was tested. While $CsSnX_3$ NCs solar cells showed a 40% efficiency decay after 16 days, the efficiency decay of $MAPbI_3$ solar cell was 70%.[63]

The observed performance is very encouraging towards the development of lead-free inorganic solar cells. Indeed, the 12.96% efficiency obtained with $CsSnI_3$ QRs is the best result for non-toxic perovskite NCs reported to date, surpasses the efficiency obtained with bulk $CsSnI_3$ (7.5%),[48] and is very close to the efficiency delivered by analogous lead-perovskite NCs devices (16%).

In this former case, $CsPbI_3$ NCs were treated with ZnI_2 to prevent iodine vacancies, which enhanced the stability.[41] The loss in efficiency observed in $CsSnI_3$ NCs devices after 4–5 days, which might be related to Sn^{2+} oxidation, can compromise their commercialization. The addition of an antioxidant agent, as commented in the previous example, or ZnI_2 treatment like in $CsPbI_3$ NCs, could be solutions to improve device stability.

$CH_3NH_3SnBr_{3-x}I_x$ nanocrystals

H. Xu *et al.* reported a method to synthesize $MASnBr_{3-x}I_x$ ($x = 0$–3) perovskite NCs and their use as light absorbers in DSSCs. The synthesis of $MASnBr_{3-x}I_x$ NCs was performed using a hot-injection method and $SnBr_2$, SnI_2 and MABr as precursors. The NCs were stabilized with oleic acid and oleylamine as capping ligands. Different halide ratios were tested: $MASnBr_3$, $MASnBr_2I$, $MASnBrI_2$ and $MASnI_3$, showing a band gap of 2.3, 2.0, 1.8 and 1.5 eV, respectively. Nanocrystals were spin-coated on top of a mesoscopic TiO_2 anode, I^-/I_3^- was used as electrolyte, and Pt as counter electrode. The PCE of the devices is collected in Table 2 with $MASnBr_2I$ showing the best efficiency.[64]

Electrochemical impedance spectra (EIS) showed that the resistance between the electrolyte and the NCs–TiO_2 interface was much higher than for state-of-the-art DSSCs, which might be due to the presence of long chain molecules such as oleylamine around the perovskite NCs. In order to improve electron extraction, TiO_2 interface was further decorated with graphene quantum dots reaching an efficiency of 0.60%. Alternatively, the introduction of the N719 dye as co-sensitizer to the $MASnBr_2I$ NCs improved the efficiency up to 8.79%,

Table 2 Band gap (E_g) and power conversion efficiency (PCE) for different $MASnBr_{3-x}I_x$ NCs. Extracted from ref. 64

NCs	E_g (eV)	PCE (%)
$MASnBr_3$	2.3	0.155
$MASnBr_2I$	2.0	0.322
$MASnBrI_2$	1.8	0.202
$MASnI_3$	1.5	0.106

which is higher than the efficiency delivered by N719 alone (7.28%).[65] As a preliminary result, an efficiency of 8.79% is very promising especially taking into account that state-of-the-art DSSCs show record efficiencies of 14.3%.[66]

To further improve these results some modifications could be introduced. For instance, great efficiencies have been achieved by substituting the I^-/I_3^- electrolyte by Co^{2+}/Co^{3+} electrolyte,[67] or using spiro-OMeTAD as HTL.[5,38,68] Capping ligands are another important parameter since, as commented above, the presence of long chain ligands is detrimental for device efficiency. Moreover, it has been demonstrated that the nature of the capping ligands will influence the interaction between the perovskite NCs and the dye or the TiO_2 interface, therefore the use of shorter or more adequate ligands could improve the device efficiency.[69] Not only that, if co-sensitization is the key to boost performance, other dyes such as Ru complex N3 have also shown improvements combined with other NCs DSSCs.[70]

Summary

According to the cell performance parameters of the different studies introducing tin-perovskite NCs in solar cells (Table 3), the most interesting approach seems to be the solvothermal synthesis of $CsSnX_3$ rod-shaped nanocrystals and the use of TiO_2 as ETL and spiro-OMeTAD as HTL, that delivers a maximum efficiency (approx. 13%).[63] The comparison of the V_{oc} found in this study for $CsSnI_3$ (0.87 V) with the value found for $CsSnI_3$ in ref. 58 (0.42 V) points to a non-optimum energy alignment among the active material and the transport layers in the latter.

In the case of the hybrid $MASnBr_{3-x}I_x$ perovskites, the low currents obtained in the DSSC devices point to an inefficient charge transfer between the NCs–TiO_2 interface and the electrolyte. As commented, the substitution of the long chain organic ligands might lead to a better contact between the nanocrystals and the

electrolyte. Additionally, the introduction of these NCs in other cell configurations, like the one used in ref. 63, could provide better efficiencies and would allow a better comparison among the different materials and synthetic strategies.

Germanium-based perovskites

Germanium also belongs to group 14 in the periodic table, together with Pb and Sn, and shares the ns^2np^2 external electronic configuration ($4s^2$ for Ge^{2+}). Therefore, analogous properties close to those observed in Pb-based perovskite materials are expected but using a non-toxic relatively abundant material. In spite of this, Ge has received little attention as light absorber for solar cells, most likely because of the significant tendency of Ge^{2+} ions to oxidize to Ge^{4+}.

Some theoretical calculations have predicted promising efficiencies for Ge perovskite solar cells. For instance, 1D-Solar Cell Capacitance Simulator (1D-SCAPS) simulations estimate a 23.58% efficiency for a $CH_3NH_3GeI_3$ ($MAGeI_3$) PSC employing $CuSbS_2$ as HTL, and by introducing Shockley–Queisser maximum solar cell efficiency (S–Q) and Spectroscopic Limited Maximum Efficiency (SLME) models in DFT calculations a theoretical value of 27.9% PCE is obtained for a $CsGeI_3$ PSC.[71,72] This reflects their great optical properties and the potential application of germanium-based materials in photovoltaic devices. Based on these good results some Ge-based bulk PSCs have been fabricated. $CsGeI_3$ solar cells achieved an initial efficiency of 0.11%,[73] which was further improved up to 3% and patented by Huang et al.[74] Moreover, germanium was included in a mixed all-inorganic tin-PSC, $CsSn_{0.5}Ge_{0.5}I_3$, reaching an efficiency of 7.11% as well as enhanced stability due to the growth of a Sn-containing GeO_2 native passivation oxide layer (formed spontaneously when exposed to air).[75] Hybrid organic inorganic materials, like $MAGeI_3$, have also been tested delivering a 0.2% efficiency,[73] which was later increased up to a 0.56% by introducing a 10% of bromide in the composition ($MAGeI_{2.7}Br_{0.3}$).[76] Additionally, germanium has been used in a formamidinium antimony-PSC ($FA_4GeSbCl_{12}$) achieving a 4.7% efficiency.[77] Finally, a FA and MA Ge-doped Sn perovskite, $FA_{0.75}MA_{0.25}Sn_{1-x}Ge_xI_3$, was used as active layer leading to an efficiency of 7.9% when a 5% of Ge was present.[78] In summary, thin-film photovoltaics using Ge-perovskites are scarce and have reached efficiency values up to 3%; however, when combined with other non-toxic elements such as Sn or Sb, the efficiency is greatly increased, attributed to an improved passivation, suppression of recombination, and reduction of trap states, which improve carrier dynamics.[75,77,78]

As the oxidation of Ge^{2+} to Ge^{4+} in air is quite straightforward, reports of Ge perovskite NCs applied in photovoltaics are limited, as spontaneous oxidation is favoured in NCs because of their high surface/volume ratio. Although there are some reports of Ge perovskite NCs synthesis,[42,79] very few address their use in solar cells.[80]

$CsGeX_3$ nanocrystals (X = Cl, Br, I)

A simple solvothermal method was proposed to synthesize rod-shaped $CsGeX_3$ (X = Cl, Br, I) NCs using diethylenetriamine

Table 3 Summary of solar cell performance parameters of champion devices fabricated with tin-based perovskite nanocrystals. Open circuit voltage (V_{oc}), short circuit current density (J_{sc}), fill factor (FF), and power conversion efficiency (PCE)

NCs	V_{oc} (V)	J_{sc} (mA cm^{-2})	FF	PCE (%)	Ref.
$CsSnI_3$ + TPPi	0.42	23.79	0.42	4.13	58
$CsSnCl_3$	0.87	19.82	0.56	9.66	63
$CsSnBr_3$	0.85	21.23	0.58	10.46	63
$CsSnI_3$	0.87	23.2	0.65	12.96	63
$MASnBr_3$	0.53	0.62	0.48	0.155	64
$MASnBr_2I$	0.56	0.87	0.65	0.322	64
$MASnBrI_2$	0.52	0.70	0.56	0.202	64
$MASnI_3$	0.46	0.55	0.43	0.106	64

(DIEN) and TOPO as capping ligands. Fig. 4 shows the current density–voltage (J–V) curves for solar cells fabricated with the different halides, using TiO_2 as electron transport layer and spiro-OMeTAD as hole transport layer.

Results are shown in Table 4. Iodide QRs show the highest efficiency, closely followed by the bromide ones, probably due to their more adequate band gap.[80] The obtained currents are very encouraging and the strategies to improve efficiency should focus on improving V_{oc} and FF. In that sense, it would be interesting to explore alternative transport layers. In any case this result is very promising since the 5% efficiency obtained with $CsGeI_3$ NCs surpasses the efficiency obtained in $CsGeI_3$ bulk PSC (0.11% and 3%).[73,74] However, there is room for improvement; devices based on other inorganic perovskite NCs such as $CsPbI_3$ NCs achieved an efficiency up to 16.07% and the analogous Sn NCs ($CsSnI_3$ QRs) offered an efficiency of 12.96%.[63] As stated above, Ge^{2+} inert pair effect is less prominent than in Sn or Pb; therefore, its tendency to oxidize to Ge^{4+} is greater. This instability is a major concern for Ge-based perovskites and one possible solution would be the addition of antioxidant compounds. As described in the previous section, this strategy has successfully been explored in Sn materials where the addition of edamine, pyrazine, triphenyl phosphite, or SnI_2 excess improved the device stability.[47,49,58] Moreover, the use of $CuSbS_2$ as HTL instead of spiro-OMeTAD could be a better match for this material.[71]

Bismuth-based perovskites

Bismuth perovskites have been studied as potential substitutes of lead perovskites in solar cells. Bismuth(III) is a trivalent metal cation isoelectronic with lead(II) (both Bi^{3+} and Pb^{2+} have a $6s^2 6p^0$ electronic configuration) and their compounds share similar properties. In spite of being a heavy metal, it is considered as a non-toxic element even used in biomedicine.[81] Additionally bismuth materials have shown exceptional stability in ambient conditions. Bismuth perovskite solar cells maintained their composition and structural integrity after 72 h under moisture conditions at 100 °C, while Pb devices showed decomposition after 72 h in air at 60 °C.[82] Not only that, even bismuth doping of lead perovskites induce an improvement in stability. Fan Bai et al. reported a mixed perovskite α-$CsPb_{1-x}Bi_xI_3$ with an efficiency of 13.21% and a significant improvement of the durability (around 70% of the efficiency is maintained after 168 h).[83]

Different examples of bismuth-perovskite solar cells have been reported, such as $(CH_3NH_3)_3Bi_2I_9$ ($MA_3Bi_2I_9$) PSC fabricated by vapour deposition that achieved a 3.17% efficiency.[84] Additionally, all-inorganic perovskite solar cells like $Cs_3Bi_2I_9$, employing CuI as HTL and TiO_2 as ETL, led to an efficiency of 3.20%.[85] One year later, using ZnO instead of TiO_2, the efficiency was enhanced up to 9.20%.[86] BiI_3 was tested in thin-film solar cell leading to an efficiency of 1.21%[15] that has recently increased to 1.33% in a device with V_2O_5 as HTL and ZnO as ETL.[87] Other Bi-based perovskite materials are the silver bismuth iodide family, with a maximum efficiency of 4.3% obtained for Ag_3BiI_6,[28] or double perovskites ($A_2M^+M^{3+}X_6$), where one M^+ and one M^{3+} cations substitute two Pb^{2+} cations. $Cs_2AgBiBr_6$ films deposited by vacuum sublimation have delivered an efficiency of 1.41%, and 2.51% for films obtained by spin-coating onto a TiO_2 layer.[88] Recently, the introduction of a N719 dye interlayer between the $Cs_2AgBiBr_6$ and spiro-OMeTAD layers has shown to enhance the efficiency to 2.84%, also improving the stability under ambient conditions.[89] Finally, a bulk heterojunction perovskite solar cell with the photoactive layer consisting of $Cs_3Bi_2I_9$ and $Ag_3Bi_2I_9$ has led to a 3.6% efficiency.[90] Although these are promising results, bismuth-perovskites suffer from the presence of a high number of defects that induce non-radiative recombination of charges and decrease the power conversion efficiency.[10,91]

In the last years several bismuth perovskite NCs have been synthesized and their optical properties have been studied showing good absorption and emissive properties, with PLQY as high as 62%.[92] However, in spite of these promising optical properties, only a few examples of Bi-perovskite NCs have been used to fabricate solar devices. In this section, studies focusing on $Cs_3Bi_2I_9$, $Cs_2AgBiBr_6$, $KBaTeBiO_6$ NCs, and $Bi_{13}S_{18}I_2$ nanorods are discussed.

$Cs_3Bi_2I_9$ nanocrystals

$A_3B_2X_9$ NCs (where A = CH_3NH_3, Cs, or Rb, B = Bi or Sb, and X = Cl, Br, or I) were synthesized using a colloidal hot-injection method in which 1-dodecanol was added to act as solvent and capping agent. $Cs_3Bi_2I_9$ NCs, with a band gap around 2 eV, were used to fabricate solar cells with SnO_2 as ETL and spiro-OMeTAD as HTL. The efficiency was 0.0103%,[93] which is far from the 9.2% of the bulk analogue.[86] However, in the bulk analogue, the PCE was enhanced by substituting spiro-OMeTAD by CuI as HTL.[85,86] By changing the HTL or the ETL in $Cs_3Bi_2I_9$ NCs solar cells the efficiency could also be improved.


Fig. 4 (A) J–V characteristics of $CsGeI_3$ (blue), $CsGeBr_3$ (red), and $CsGeCl_3$ (black) solar cells. The inset shows a picture of a solar cell. (B) Incident Photon-to-electron Conversion Efficiency (IPCE) of $CsGeX_3$ perovskite devices with different halides. Reproduced from ref. 80 with permission from the Royal Society of Chemistry. (RSC, RSC Advances).

Table 4 Band gap (E_g) of $CsGeX_3$ (X = Cl, Br, I) NCs and solar cell performance parameters of devices fabricated with them. Band gap values have been calculated from absorption spectra. Extracted from ref. 80

QRs	E_g (eV)	V_{oc} (V)	J_{sc} (mA cm^{-2})	FF	PCE (%)
$CsGeCl_3$	2	0.35	18.57	0.40	2.57
$CsGeBr_3$	1.9	0.49	19.49	0.52	4.92
$CsGeI_3$	1.8	0.52	18.78	0.51	4.94

Moreover, the dodecanol chains on the surface of the NCs could be replaced following a ligand exchange process, which may improve the optical properties and charge transport.[4,94,95]

$Cs_2AgBiBr_6$ nanocrystals

Employing a colloidal synthesis route, $Cs_2AgBiBr_6$ double perovskite NCs were synthesized and deposited as thin-films, obtaining stable absorbing layers for PSC. The colloidal stability can be attributed to the surface passivation treatment with oleylamine, oleic acid, and trioctylphosphine. These ligands were substituted by bromide ions after treatment with TBAB (tetrabutyl-ammonium bromide) during film fabrication. The $Cs_2AgBiBr_6$ NCs absorber layer, indirect band gap of 2.28 eV, was sandwiched between compact TiO_2 and spiro-OMeTAD as the electron and hole transport material, respectively. The best performing device, obtained for NCs with optimum size (7.6 nm), exhibited a 0.46% efficiency. Additionally, larger NCs were also synthesized and tested obtaining a lower value of 0.028%, attributed to problems in the morphology of the film.[96] These values are low when compared to previous reports for the analogous bulk material which delivered efficiencies of 2.51%. The underperformance of these devices has been attributed to the low charge carrier mobility, trap-assisted recombination and poor charge collection. More research is needed in the optimization of the energy levels between NCs and transport layers; for instance, the presence of ethylammonium has been proved to enhance the charge transport by adjusting the energy levels in Sn-based PSC.[52]

$KBaTeBiO_6$ nanocrystals

By using computational calculations, it was predicted that $KBaTeBiO_6$ (double perovskite oxide) is a potential non-toxic candidate for photovoltaic applications. The calculated maximum efficiency was around 4% for a 1 μm thick film, which could be tuned by changing the cation stoichiometry in the material. Following a simple wet-chemistry route and mixing solutions of the respective precursors, KNO_3, $Ba(NO_3)_2$, $Bi(NO_3)_3 \cdot 5H_2O$ and $Te(OH)_6$ in the adequate proportions, $KBaTeBiO_6$ NCs were obtained. The NCs (direct band gap of 1.88 eV), were dispersed in ethanol and water with and without binders (terpineol and ethyl cellulose), drop-casted on top of a TiO_2 electrode, and used as sensitizer in a DSSC. The average efficiency obtained was 0.04%, with a best efficiency of 0.06% for the material dispersed without binders.[97] This may appear as a very low value, especially as compared to the 14.3% record efficiency for DSSCs,[66] and to the 6.5% achieved employing $MAPbI_3$ as sensitizer in DSSC.[98] However, $KBaTeBiO_6$ NCs show better material stability than bismuth-based halide perovskites and their solar cells show similar performance to those based on high quality thin films of other inorganic oxide perovskites. Furthermore, the study and control of defects including oxygen vacancies, cation nonstoichiometry, and disorder in $KBaTeBiO_6$ will be a crucial task to achieve optimal performance from these semiconductors.

$Bi_{13}S_{18}I_2$ nanocrystals

$Bi_{13}S_{18}I_2$ NCs were synthesized following a solvothermal method, mixing the precursors BiI_3, thiourea (CH_4N_2S), and CH_3NH_3I (MAI) in ethylene glycol at 195 °C in a 2:4:3 ratio, respectively. The obtained nanorods had a diameter of 50 nm and a band gap of 0.75 eV,[100] a value smaller than the ideal band gap for a single p–n junction solar cell.[99]

$Bi_{13}S_{18}I_2$ nanorods were used as sensitizer in DSSC (Fig. 5A), and a maximum efficiency of 0.85% was achieved, showing low variability among the 8 different devices (Fig. 5B).[100] The low PCE is due to the low current and fill factor values, which may be improved optimising the thickness of $Bi_{13}S_{18}I_2$ and TiO_2 films, or using a different electrolyte or hole transport material. Along this line, the use of polysulfide electrolytes led to better efficiencies for NCs DSSCs.[101]

Summary

Table 5 summarizes the solar cell parameters of the Bi-perovskite NCs devices. $Cs_3Bi_2I_9$ and $Cs_2AgBiBr_6$ NCs were synthesized using a colloidal synthesis that provides a precise control over the composition and size of the final material. The devices fabricated with these NCs used an almost identical solar cell structure with compact TiO_2 and spiro-OMeTAD as transport layers.[93,96] However, the device fabricated with $Cs_2AgBiBr_6$ NCs,[96] that follows a ligand exchange process, showed better currents and V_{oc}, pointing to the effectiveness of this approach in improving charge transport. A different selection of final ligands could further improve charge transport and adjust energy levels between the absorbing and transport layers, leading to better efficiencies.

$KBaTeBiO_6$ and $Bi_{13}S_{18}I_2$ NCs have been used as dyes in DSSC devices employing the same counter electrode, solar cell area (0.25 cm^2), and a similar electrolyte, based on the I^-/I_3^- couple.[97,100] The device incorporating the $KBaTeBiO_6$ NCs showed very low current probably because of the presence of defects in the crystalline structure, coming from the lack of control over the composition of the mixed oxide, and on the
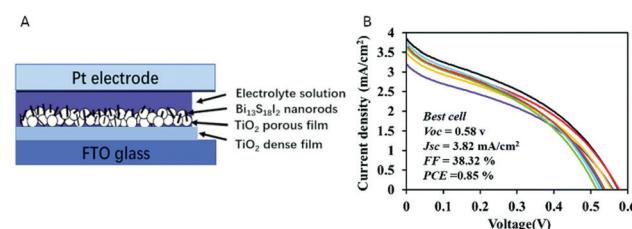
Fig. 5 (A) Scheme of the $Bi_{13}S_{18}I_2$ NCs solar cell structure. (B) J–V curves of eight $Bi_{13}S_{18}I_2$ solar cells. Reproduced from ref. 100 with permission from the Royal Society of Chemistry. (RSC, Journal of Materials Chemistry C).

Table 5 Summary of solar cell performance parameters of champion devices fabricated with bismuth-based perovskite nanocrystals. Open circuit voltage (V_{oc}), short circuit current density (J_{sc}), fill factor (FF), and power conversion efficiency (PCE)

NCs	V_{oc} (V)	J_{sc} (mA cm^{-2})	FF	PCE (%)	Ref.
$Cs_3Bi_2I_9$	0.22	0.14	0.34	0.01	93
$Cs_2AgBiBr_6$	0.80	1.17	0.49	0.46	96
$KBaTeBiO_6$	0.54	0.09	0.58	0.06	97
$Bi_{13}S_{18}I_2$	0.58	3.82	0.38	0.85	100

surface, originated by the absence of passivating agents. Better results are obtained with the $Bi_{13}S_{18}I_2$ NCs, synthesized using a simple solvothermal method. It would be interesting to explore the introduction of this material in a n–i–p solar cell structure to compare with ref. 93 and 96.

Antimony-based perovskites

Antimony belongs to the same group as bismuth and, consequently, Sb-perovskites have also been proposed as non-toxic alternative to lead-based perovskites. Like Bi^{3+}, Sb^{3+} cations are isoelectronic to Pb^{2+} and, usually, form perovskites with the formula $A_3Sb_2X_9$ (where A = MA, Cs or Rb and X = Cl, Br or I). Similarly, to Bi-perovskites, they exhibit high absorption coefficients, small effective masses (facilitating mobility) and suitable band gaps for photovoltaic applications (usually between 1 eV and 2 eV). Moreover, their properties can be tuned depending on the structure (0D or 2D layered).[102] Antimony can be a good alternative to other non-toxic materials mentioned in this text; it does not suffer from oxidation processes like Sn or Ge, and is more abundant in the earth-crust than Bi.[103] In spite of this, Sb-perovskite reports are less common than those focusing on Sn or Bi, probably because they suffer from a high presence of deep defects that act as recombination centres.[10,104]

Some bulk Sb-perovskite materials have been synthesized, characterized, and introduced as light harvesters in solar cells. In 2016, 0D methylammonium $MA_3Sb_2I_9$ thin-film solar cells were fabricated achieving a power conversion efficiency of 0.5%.[105] Two years later, it was demonstrated that 0D $MA_3Sb_2I_9$ perovskite had an indirect band gap, reduced carrier transport, and their films suffered from nonradiative recombination and it was suggested that a 2D layered structure could produce better results. This 2D-perovskite could be easily obtained by adding chloride to $MA_3Sb_2I_9$ films. Thus, 2D $MA_3Sb_2Cl_xI_{9-x}$ films were introduced in solar cells achieving an efficiency of 2.19%, the best result so far for Sb-only perovskite solar cells.[106] Another type of 2D antimony-perovskite, $Rb_3Sb_2I_9$, led to a maximum efficiency of 0.66%.[104]

In addition to these studies on bulk Sb-perovskites, antimony perovskite nanocrystals have also received some attention. $Cs_3Sb_2X_9$ (X = Cl, Br, I) NCs have been synthesized and stabilized with oleic acid and octadecene capping ligands. The photoluminescence quantum yields are 11% for $Cs_3Sb_2Cl_9$, 46% for $Cs_3Sb_2Br_9$, and 23% for $Cs_3Sb_2I_9$ NCs, and the band gaps are 3.35, 3.02, and 2.21 eV, respectively.[107] In spite of having the higher PLQY value, $Cs_3Sb_2Br_9$ NCs band gap is not optimal for solar cells. Nevertheless, the band gap could be tuned by modifying the nanocrystal diameter and, additionally, Sb-perovskites can be used for other applications. Furthermore, as discussed in the next section, $(NH_4)_3Sb_2I_xBr_{9-x}$ NCs have been used as light absorbers in solar cells.

$(NH_4)_3Sb_2I_xBr_{9-x}$ nanocrystals

$(NH_4)_3Sb_2I_xBr_{9-x}$ NCs were synthesized following an antisolvent vapor-assisted crystallization method using ethanol as solvent, considered as a low-cost, hypotoxic, and environmentally

Table 6 Band gap (E_g) of NCs and solar cell performance parameters of the solar cells fabricated with them. Extracted from ref. 108

NCs	E_g (eV)	V_{oc} (V)	J_{sc} (mA cm^{-2})	FF	PCE (%)
$(NH_4)_3Sb_2Br_9$	2.78	0.29	0.09	0.28	0.01
$(NH_4)_3Sb_2I_3Br_6$	2.66	0.67	0.20	0.44	0.06
$(NH_4)_3Sb_2I_6Br_3$	2.49	0.76	0.77	0.32	0.19
$(NH_4)_3Sb_2I_9$	2.27	1.03	1.15	0.43	0.51

friendly solvent. NCs with 54 nm diameter and different halide compositions were characterized and incorporated in photovoltaic devices. Table 6 collects the direct band gap of the NCs and the power conversion efficiencies of the solar cells fabricated with them. The structure of the devices was ITO/PEDOT:PSS/ $(NH_4)_3Sb_2I_xBr_{9-x}$ NCs/PC$_{61}$BM/Al, where PEDOT:PSS is the electron transport layer, and PC$_{61}$BM the hole transport layer. The stability of the best performing device, employing $(NH_4)_3Sb_2I_9$ NCs, was tested. The film became colourless and the device showed no performance after storage in air for 2 days, but when stored in a glovebox for 40 days, 80% of the efficiency was maintained, demonstrating that device stability can be improved *via* encapsulation.[108]

The iodide $(NH_4)_3Sb_2I_9$ NCs provided the best performance parameters, with a 0.51% efficiency, probably due to the most adequate band gap and a more optimum band alignment between the active and the transport layers. The low currents and FF point to problems in charge transport and extraction, which could be improved with a better film morphology and the use of alternative transport layers. The best efficiency is similar to the highest value obtained for Bi perovskite NCs (0.85% for $Bi_{13}S_{18}I_2$);[100] however, the different stoichiometry and composition make them hardly comparable. The efficiency obtained is still far from other tin or lead-based NCs perovskite solar cells, but close to values obtained for bulk inorganic Sb-perovskites $Rb_3Sb_2I_9$ and 0D $MA_3Sb_2I_9$ thin-films mentioned above (0.66% and 0.5% respectively), and still inferior to the best-performing antimony solar cell, 2D $MA_3Sb_2Cl_xI_{9-x}$ (2.2%). As a final remark concerning Sb-perovskites, a recent study suggests that Sb-perovskites have much deeper defects than Pb-perovskite NCs, which can reduce significantly the efficiency of the photovoltaic devices.[109]

Conclusions

Non-toxic perovskites are becoming more relevant in photovoltaics due to the raising concerns about lead toxicity. Even though the efficiencies of these non-toxic materials are slightly behind lead, they seem to be particularly appealing for specific applications such as indoor and wearable photovoltaics, where safety is of primary importance.

The efficiency of lead perovskite cells has grown from 3.8% in 2009 to current 25.5% for bulk and 16.6% for NCs. These improvements have been achieved thanks to the adjustment of the energy levels, enhanced stability, suppression of defects, surface treatments, charge transport improvement, and the use of different and more complex stoichiometries. In this sense,

complex and tailored compositions are not easily achievable for bulk perovskites where synthesis and deposition are simultaneous. On the contrary, perovskite NCs offer the advantage of separating both processes, which allows a better control over the stoichiometry of the material. Although the use of non-toxic perovskite NCs in solar cells is quite recent, they have already shown promising results surpassing in some cases the efficiency values obtained for their bulk counterparts: CsSnI$_3$ quantum rods show an efficiency of almost 13% (bulk material 7.5%), and CsGeI$_3$ NCs an efficiency close to 5% (bulk material $\approx 3\%$). It is worth mentioning that some of the best results are already close to the efficiency obtained for lead NCs (16.6%), and the stoichiometry or solar cell structure have not been optimized.

In this review, the main issues of non-toxic perovskite NCs have been addressed. Some of the materials suffer from oxidation problems (Ge, Sn) or high number of defects (Bi, Sb) that may harm the solar device performance. In this sense, more complex compositions could be a solution to some of the aforementioned problems. For example, including in the composition edamine that acts as antioxidant cation, ethylammonium that improves charge transport, or formamide which prevents non-radiative recombination. Additionally, the addition of antioxidant additives, more adequate transport layers, different cell structures, or surface passivation treatments are other possible approaches to improve performance.

Research on non-toxic perovskite NCs is a novel field, reports incorporating these NCs in solar cells are scarce, and many alternatives remain unexplored. Indeed, in the studies here summarized, each work uses a synthetic methodology and a solar cell structure making it difficult to compare among them and select the most promising approach. Still, impressive results have already been reported showing that non-toxic NCs could be candidates to substitute lead in the near future with more research in this area.

Conflicts of interest

There are no conflicts of interest to declare.

Acknowledgements

References

1 NREL, Best Research-Cell Efficiency Chart, 2020.

2 G. H. Carey, A. L. Abdelhady, Z. Ning, S. M. Thon, O. M. Bakr and E. H. Sargent, *Chem. Rev.*, 2015, **115**, 12732.

3 H. Lu, Z. Huang, M. S. Martinez, J. C. Johnson, J. M. Luther and M. C. Beard, *Energy Environ. Sci.*, 2020, **13**, 1347.

4 P. R. Brown, D. Kim, R. R. Lunt, N. Zhao, M. G. Bawendi, J. C. Grossman and V. Bulović, *ACS Nano*, 2014, **8**, 5863.

5 M. Hao, Y. Bai, S. Zeiske, L. Ren, J. Liu, Y. Yuan, N. Zarrabi, N. Cheng, M. Ghasemi, P. Chen, M. Lyu, D. He, J. H. Yun, Y. Du, Y. Wang, S. Ding, A. Armin, P. Meredith, G. Liu, H. M. Cheng and L. Wang, *Nat. Energy*, 2020, **5**, 79.

6 H. Yang, Y. Zhang, K. Hills-Kimball, Y. Zhou and O. Chen, *Sustainable Energy Fuels*, 2018, **2**, 2381.

7 D. B. Mitzi, *J. Chem. Soc., Dalton Trans.*, 2001, 1.

8 X. Li, J. Wu, S. Wang and Y. Qi, *Chem. Lett.*, 2019, **48**, 989.

9 S. A. Bretschneider, F. Laquai and M. Bonn, *J. Phys. Chem. C*, 2017, **121**, 11201.

10 A. M. Ganose, C. N. Savory and D. O. Scanlon, *Chem. Commun.*, 2017, **53**, 20.

11 J. Bisquert and E. J. Juarez-Perez, *J. Phys. Chem. Lett.*, 2019, **10**, 5889.

12 Y. Deng, L. Jiang, L. Xu, X. Hao, S. Zhang, M. Xu, P. Zhu, S. Fu, Y. Liang, H. Yin, X. Liu, L. Bai, H. Jiang and H. Liu, *Ecotoxicol. Environ. Saf.*, 2019, **171**, 281.

13 Z. Xiao, Z. Song and Y. Yan, *Adv. Mater.*, 2019, **31**, 1.

14 Q. Zhang and Y. Yin, *ACS Cent. Sci.*, 2018, **4**, 668.

15 C. Wu, Q. Zhang, G. Liu, Z. Zhang, D. Wang, B. Qu, Z. Chen and L. Xiao, *Adv. Energy Mater.*, 2019, 1902496.

16 X. Zhao and N. G. Park, *Photonics*, 2015, **2**, 1139.

17 R. E. Brandt, J. R. Poindexter, P. Gorai, R. C. Kurchin, R. L. Z. Hoye, L. Nienhaus, M. W. B. Wilson, J. A. Polizzotti, R. Sereika, R. Žaltauskas, L. C. Lee, J. L. Macmanus-Driscoll, M. Bawendi, V. Stevanović and T. Buonassisi, *Chem. Mater.*, 2017, **29**, 4667.

18 L. C. Lee, T. N. Huq, J. L. Macmanus-Driscoll and R. L. Z. Hoye, *APL Mater.*, 2018, **6**, 084502.

19 A. Babayigit, H.-G. Boyen and B. Conings, *MRS Energy Sustainability*, 2018, **5**, 15.

20 P. Su, Y. Liu, J. Zhang, C. Chen, B. Yang, C. Zhang and X. Zhao, *J. Phys. Chem. Lett.*, 2020, **11**, 2812.

21 T. Miyasaka, A. Kulkarni, G. M. Kim, S. Öz and A. K. Jena, *Adv. Energy Mater.*, 2020, **10**, 1.

22 Y. Peng, T. N. Huq, J. Mei, L. Portilla, R. A. Jagt, L. G. Occhipinti, J. L. MacManus-Driscoll, R. L. Z. Hoye and V. Pecunia, *Adv. Energy Mater.*, 2021, **11**, 2002761.

23 S. A. Hashemi, S. Ramakrishna and A. G. Aberle, *Energy Environ. Sci.*, 2020, **13**, 685.

24 X. Hou, Y. Wang, H. K. H. Lee, R. Datt, N. Uslar Miano, D. Yan, M. Li, F. Zhu, B. Hou, W. C. Tsoi and Z. Li, *J. Mater. Chem. A*, 2020, **8**, 21503.

25 M. Lyu, J. H. Yun, P. Chen, M. Hao and L. Wang, *Adv. Energy Mater.*, 2017, **7**, 1602512.

26 L. Liang and P. Gao, *Adv. Sci.*, 2017, **5**, 1700331.

27 S. Attique, N. Ali, S. Ali, R. Khatoon, N. Li, A. Khesro, S. Rauf, S. Yang and H. Wu, *Adv. Sci.*, 2020, **7**, 1903143.

28 I. Turkevych, S. Kazaoui, E. Ito, T. Urano, K. Yamada, H. Tomiyasu, H. Yamagishi, M. Kondo and S. Aramaki, *ChemSusChem*, 2017, **10**, 3754.

29 D. Shi, Y. Zeng and W. Shen, *Sci. Rep.*, 2015, **5**, 1.

30 T. Saga, *NPG Asia Mater.*, 2010, **2**, 96.

31 W. Ke, C. C. Stoumpos and M. G. Kanatzidis, *Adv. Mater.*, 2019, **31**, 1803230.

32 N. C. Miller and M. Bernechea, *APL Mater.*, 2018, **8**, 084503.

33 A. Swarnkar, V. K. Ravi and A. Nag, *ACS Energy Lett.*, 2017, **2**, 1089.

34 H. Siddiqui, *Mater. Lett.*, 2019, **249**, 99.

35 S. Ghosh and B. Pradhan, *ChemNanoMat*, 2019, **5**, 300.

36 A. Kojima, K. Teshima, Y. Shirai and T. Miyasaka, *J. Am. Chem. Soc.*, 2009, **131**, 6050.

37 J. H. Im, C. R. Lee, J. W. Lee, S. W. Park and N. G. Park, *Nanoscale*, 2011, **3**, 4088.

38 H. S. Kim, C. R. Lee, J. H. Im, K. B. Lee, T. Moehl, A. Marchioro, S. J. Moon, R. Humphry-Baker, J. H. Yum, J. E. Moser, M. Grätzel and N. G. Park, *Sci. Rep.*, 2012, **2**, 591.

39 A. Swarnkar, A. R. Marshall, E. M. Sanehira, B. D. Chernomordik, D. T. Moore, J. A. Christians, T. Chakrabarti and J. M. Luther, *Science*, 2016, **354**, 92.

40 K. Ji, J. Yuan, F. Li, Y. Shi, X. Ling, X. Zhang, Y. Zhang, H. Lu, J. Yuan and W. Ma, *J. Mater. Chem. A*, 2020, **8**, 8104.

41 L. Zhang, C. Kang, G. Zhang, Z. Pan, Z. Huang, S. Xu, H. Rao, H. Liu, S. Wu, X. Wu, X. Li, Z. Zhu, X. Zhong and A. K.-Y. Jen, *Adv. Funct. Mater.*, 2020, 2005930.

42 D. Carolan, *Prog. Mater. Sci.*, 2017, **90**, 128.

43 S. F. Hoefler, G. Trimmel and T. Rath, *Monatsh. Chem.*, 2017, **148**, 795.

44 A. Abate, *Joule*, 2017, **1**, 659.

45 W. Li, J. J. Li, J. J. Li, J. Fan, Y. Mai and L. Wang, *J. Mater. Chem. A*, 2016, **4**, 17104.

46 T. C. Jellicoe, J. M. Richter, H. F. J. Glass, M. Tabachnyk, R. Brady, S. E. Dutton, A. Rao, R. H. Friend, D. Credgington, N. C. Greenham and M. L. Böhm, *J. Am. Chem. Soc.*, 2016, **138**, 2941.

47 T. Bin Song, T. Yokoyama, S. Aramaki and M. G. Kanatzidis, *ACS Energy Lett.*, 2017, **2**, 897.

48 T. Ye, K. Wang, Y. Hou, D. Yang, N. Smith, B. Magill, J. Yoon, R. R. H. H. Mudiyanselage, G. A. Khodaparast, K. Wang and S. Priya, *J. Am. Chem. Soc.*, 2021, **143**, 4319–4328.

49 S. J. Lee, S. S. Shin, Y. C. Kim, D. Kim, T. K. Ahn, J. H. Noh, J. Seo and S. Il Seok, *J. Am. Chem. Soc.*, 2016, **138**, 3974.

50 S. Shao, J. Liu, G. Portale, H.-H. Fang, G. R. Blake, G. H. ten Brink, L. J. A. Koster and M. A. Loi, *Adv. Energy Mater.*, 2018, **8**, 1702019.

51 M. A. Kamarudin, D. Hirotani, Z. Wang, K. Hamada, K. Nishimura, Q. Shen, T. Toyoda, S. Iikubo, T. Minemoto, K. Yoshino and S. Hayase, *J. Phys. Chem. Lett.*, 2019, **10**, 5277.

52 K. Nishimura, M. A. Kamarudin, D. Hirotani, K. Hamada, Q. Shen, S. Iikubo, T. Minemoto, K. Yoshino and S. Hayase, *Nano Energy*, 2020, **74**, 104858.

53 W. Ke, C. C. Stoumpos, I. Spanopoulos, L. Mao, M. Chen, M. R. Wasielewski and M. G. Kanatzidis, *J. Am. Chem. Soc.*, 2017, **139**, 14800.

54 Z. Zhao, F. Gu, Y. Li, W. Sun, S. Ye, H. Rao, Z. Liu, Z. Bian and C. Huang, *Adv. Sci.*, 2017, **4**, 1700204.

55 A. Kaltzoglou, M. Antoniadou, A. G. Kontos, C. C. Stoumpos, D. Perganti, E. Siranidi, V. Raptis, K. Trohidou, V. Psycharis, M. G. Kanatzidis and P. Falaras, *J. Phys. Chem. C*, 2016, **120**, 11777.

56 X. Qiu, B. Cao, S. Yuan, X. Chen, Z. Qiu, Y. Jiang, Q. Ye, H. Wang, H. Zeng, J. Liu and M. G. Kanatzidis, *Sol. Energy Mater. Sol. Cells*, 2017, **159**, 227.

57 X. Qiu, Y. Jiang, H. Zhang, Z. Qiu, S. Yuan, P. Wang and B. Cao, *Phys. Status Solidi RRL*, 2016, **10**, 587.

58 Y. Wang, J. Tu, T. Li, C. Tao, X. Deng and Z. Li, *J. Mater. Chem. A*, 2019, **7**, 7683.

59 F. Zhang, H. Zhong, C. Chen, X. G. Wu, X. Hu, H. Huang, J. Han, B. Zou and Y. Dong, *ACS Nano*, 2015, **9**, 4533.

60 C. H. M. Chuang, P. R. Brown, V. Bulović and M. G. Bawendi, *Nat. Mater.*, 2014, **13**, 796.

61 R. Abargues, J. Navarro, P. J. Rodríguez-Cantó, A. Maulu, J. F. Sánchez-Royo and J. P. Martínez-Pastor, *Nanoscale*, 2019, **11**, 1978.

62 A. Salant, M. Shalom, Z. Tachan, S. Buhbut, A. Zaban and U. Banin, *Nano Lett.*, 2012, **12**, 2095.

63 L. J. Chen, C. R. Lee, Y. J. Chuang, Z. H. Wu and C. Chen, *J. Phys. Chem. Lett.*, 2016, **7**, 5028.

64 H. Xu, H. Yuan, J. Duan, Y. Zhao, Z. Jiao and Q. Tang, *Electrochim. Acta*, 2018, **282**, 807.

65 Z. Wu, Y. Wei, Z. An, X. Chen and P. Chen, *Bull. Korean Chem. Soc.*, 2014, **35**, 1449.

66 K. Kakiage, Y. Aoyama, T. Yano, K. Oya, J. I. Fujisawa and M. Hanaya, *Chem. Commun.*, 2015, **51**, 15894.

67 S. Mathew, A. Yella, P. Gao, R. Humphry-baker, B. F. E. Curchod, N. Ashari-astani, I. Tavernelli, U. Rothlisberger, K. Nazeeruddin and M. Grätzel, *Nat. Chem.*, 2014, **6**, 242.

68 S. S. Mali, C. S. Shim and C. K. Hong, *NPG Asia Mater.*, 2015, **7**, e208.

69 S. Giménez, A. L. Rogach, A. A. Lutich, D. Gross, A. Poeschl, A. S. Susha, I. Mora-Seró, T. Lana-Villarreal and J. Bisquert, *J. Appl. Phys.*, 2011, **110**, 014314.

70 T. Ganesh, R. S. Mane, G. Cai, J. H. Chang and S. H. Han, *J. Phys. Chem. C*, 2009, **113**, 7666.

71 A. Hima and N. Lakhdar, *Opt. Mater.*, 2020, **99**, 109607.

72 J. Qian, B. Xu and W. Tian, *Org. Electron.*, 2016, **37**, 61.

73 T. Krishnamoorthy, H. Ding, C. Yan, W. L. Leong, T. Baikie, Z. Zhang, M. Sherburne, S. Li, M. Asta, N. Mathews and S. G. Mhaisalkar, *J. Mater. Chem. A*, 2015, **3**, 23829.

74 C. Huang, X. C. X. C. Yan, G. G. Cui, Z. Z. Liu, S. S. Pang and H. Xu, *Novel Germanium-Containing Perovskite Material and Solar Cell Comprising Same*, CN 201410173750, 2014.

75 M. Chen, M. G. Ju, H. F. Garces, A. D. Carl, L. K. Ono, Z. Hawash, Y. Zhang, T. Shen, Y. Qi, R. L. Grimm, D. Pacifici, X. C. Zeng, Y. Zhou and N. P. Padture, *Nat. Commun.*, 2019, **10**, 1.

76 I. Kopacic, B. Friesenbichler, S. F. Hoefler, B. Kunert, H. Plank, T. Rath and G. Trimmel, *ACS Appl. Energy Mater.*, 2018, **1**, 343.

77 W. B. Dai, S. Xu, J. Zhou, J. Hu, K. Huang and M. Xu, *Sol. Energy Mater. Sol. Cells*, 2019, **192**, 140.

78 C. H. Ng, K. Nishimura, N. Ito, K. Hamada, D. Hirotani, Z. Wang, F. Yang, S. likubo, Q. Shen, K. Yoshino, T. Minemoto and S. Hayase, *Nano Energy*, 2019, **58**, 130.

79 X. Wu, W. Song, Q. Li, X. Zhao, D. He and Z. Quan, *Chem. – Asian J.*, 2018, **13**, 1654.

80 L. J. Chen, *RSC Adv.*, 2018, **8**, 18396.

81 Y. Yang, R. Ouyang, L. Xu, N. Guo, W. Li, K. Feng, L. Ouyang, Z. Yang, S. Zhou and Y. Miao, *J. Coord. Chem.*, 2015, **68**, 379.

82 A. H. Slavney, T. Hu, A. M. Lindenberg and H. I. Karunadasa, *J. Am. Chem. Soc.*, 2016, **138**, 2138.

83 Y. Hu, F. Bai, X. Liu, Q. Ji, X. Miao, T. Qiu and S. Zhang, *ACS Energy Lett.*, 2017, **2**, 2219.

84 S. M. Jain, D. Phuyal, M. L. Davies, M. Li, B. Philippe, C. De Castro, Z. Qiu, J. Kim, T. Watson, W. C. Tsoi, O. Karis, H. Rensmo, G. Boschloo, T. Edvinsson and J. R. Durrant, *Nano Energy*, 2018, **49**, 614.

85 F. Bai, Y. Hu, Y. Hu, T. Qiu, X. Miao and S. Zhang, *Sol. Energy Mater. Sol. Cells*, 2018, **184**, 15.

86 J. H. Heo, M. H. Lee, D. H. Song, N. M. S. Aung, J.-J. Lee, C. E. Song, K.-H. Hong and S. Hyuk Im, *J. Nanoelectron. Optoelectron.*, 2019, **13**, 1764.

87 Y. Wang, X. Shi, G. Wang, J. Tong and D. Pan, *J. Mater. Chem. C*, 2020, **8**, 14066.

88 F. Igbari, R. Wang, Z. K. Wang, X. J. Ma, Q. Wang, K. L. Wang, Y. Zhang, L. S. Liao and Y. Yang, *Nano Lett.*, 2019, **19**, 2066.

89 X. Yang, Y. Chen, P. Liu, H. Xiang, W. Wang, R. Ran, W. Zhou and Z. Shao, *Adv. Funct. Mater.*, 2020, **30**, 2001557.

90 W. Hu, X. He, Z. Fang, W. Lian, Y. Shang, X. Li, W. Zhou, M. Zhang, T. Chen, Y. Lu, L. Zhang, L. Ding and S. Yang, *Nano Energy*, 2020, **68**, 104362.

91 B. W. Park, B. Philippe, X. Zhang, H. Rensmo, G. Boschloo and E. M. J. Johansson, *Adv. Mater.*, 2015, **27**, 6806.

92 Y. Lou, M. Fang, J. Chen and Y. Zhao, *Chem. Commun.*, 2018, **54**, 3779.

93 M. M. Yao, C. H. Jiang, J. S. Yao, K. H. Wang, C. Chen, Y. C. Yin, B. S. Zhu, T. Chen and H. Bin Yao, *Inorg. Chem.*, 2019, **58**, 11807.

94 M. Soreni-Harari, N. Yaacobi-Gross, D. Steiner, A. Aharoni, U. Banin, O. Millo and N. Tessler, *Nano Lett.*, 2008, **8**, 678.

95 M. Leng, Y. Yang, Z. Chen, W. Gao, J. Zhang, G. Niu, D. Li, H. Song, J. Zhang, S. Jin and J. Tang, *Nano Lett.*, 2018, **18**, 6076.

96 R. Ahmad, G. V. Nutan, D. Singh, G. Gupta, U. Soni, S. Sapra and R. Srivastava, *Nano Res.*, 2021, **14**, 1126.

97 A. S. Thind, S. Kavadiya, M. Kouhnavard, R. Wheelus, S. B. Cho, L. Y. Lin, C. Kacica, H. K. Mulmudi, K. A. Unocic, A. Y. Borisevich, G. Pilania, P. Biswas and R. Mishra, *Chem. Mater.*, 2019, **31**, 4769.

98 J. H. Im, C. R. Lee, J. W. Lee, S. W. Park and N. G. Park, *Nanoscale*, 2011, **3**, 4088.

99 W. Shockley and H. J. Queisser, *J. Appl. Phys.*, 1961, **32**, 510.

100 S. Li, L. Xu, X. Kong, T. Kusunose, N. Tsurumachi and Q. Feng, *J. Mater. Chem. C*, 2020, **8**, 3821.

101 S. S. Mali, J. V. Patil, H. Kim, P. S. Patil and C. K. Hong, *Nanomaterials for Solar Cell Applications*, Elsevier, 2019, pp. 513–555.

102 B. Saparov, F. Hong, J. P. Sun, H. S. Duan, W. Meng, S. Cameron, I. G. Hill, Y. Yan and D. B. Mitzi, *Chem. Mater.*, 2015, **27**, 5622.

103 N. N. Greenwood and A. Earnshaw, *Chemical Element*, Elsevier, 1997, pp. 547–599.

104 P. C. Harikesh, H. K. Mulmudi, B. Ghosh, T. W. Goh, Y. T. Teng, K. Thirumal, M. Lockrey, K. Weber, T. M. Koh, S. Li, S. Mhaisalkar and N. Mathews, *Chem. Mater.*, 2016, **28**, 7496.

105 J. C. Hebig, I. Kühn, J. Flohre and T. Kirchartz, *ACS Energy Lett.*, 2016, **1**, 309.

106 F. Jiang, D. Yang, Y. Jiang, T. Liu, X. Zhao, Y. Ming, B. Luo, F. Qin, J. Fan, H. Han, L. Zhang and Y. Zhou, *J. Am. Chem. Soc.*, 2018, **140**, 1019.

107 J. Zhang, Y. Yang, H. Deng, U. Farooq, X. Yang, J. Khan, J. Tang and H. Song, *ACS Nano*, 2017, **11**, 9294.

108 C. Zuo and L. Ding, *Angew. Chem., Int. Ed.*, 2017, **56**, 6528.

109 J. Pal, S. Manna, A. Mondal, S. Das, K. V. Adarsh and A. Nag, *Angew. Chem., Int. Ed.*, 2017, **56**, 14187.